SIMULTANEOUS NONLOCAL LOW-RANK AND DEEP PRIORS FOR POISSON DENOISING

Zhiyuan Zha[1], *Bihan Wen*[1*], *Xin Yuan*[2], *Jiantao Zhou*[3] *and Ce Zhu*[4]

[1]School of Electrical & Electronic Engineering, Nanyang Technological University, Singapore 639798.
[2]Nokia Bell Labs, 600 Mountain Avenue, Murray Hill, NJ, 07974, USA.
[3]Department of Computer and Information Science, University of Macau, Macau 999078, China.
[4]School of Information and Communication Engineering,
University of Electronic Science and Technology of China, Chengdu, 611731, China.

ABSTRACT

Poisson noise is a common electronic noise, which has widely occurred in various photo-limited imaging systems. However, due to signal-dependent and multiplicative characteristics for Poisson noise, Poisson denoising is still an open problem. In this paper, we propose a novel approach using simultaneous nonlocal low-rank and deep priors (SNLDP) for Poisson denoising. The proposed SNLDP simultaneously employs nonlocal self-similarity and deep image priors under the hybrid plug and play framework, which comprises multiple pairs of complementary priors, namely, *nonlocal* and *local*, *shallow* and *deep*, and *internal* and *external*. To make the optimization tractable, an effective alternating direction method of multiplier (ADMM) algorithm under the alternative minimization framework is provided to solve the proposed SNLDP-based Poisson denoising problem. Experimental results demonstrate the superiority of the proposed SNLDP over many popular or state-of-the-art Poisson denoising algorithms in terms of quantitative and visual perception.

***Index Terms*—** Poisson denoising, nonlocal self-similarity, deep prior, hybrid plug and play, optimization.

1. INTRODUCTION

Image denoising is a fundamental problem in image processing, and when we mentioned the image denoising task, it usually refers to removing additive white Gaussian noise (AWGN) within independent distribution in images [1]. However, in many imaging applications, such as astronomy [2] and spectral [3], degradation is caused by Poisson noise that is acquired by counting the number of photons incident on the sensors [4–7]. Different from traditional AWGN, Poisson noise is signal-dependent [7]. Therefore, the standard Gaussian denoising algorithms cannot be directly used to suppress Poisson noise, leading to Poisson denoising being still an open problem.

Poisson denoising methods are usually classified into two categories: indirect methods [4, 10, 11] and direct methods [5–7, 12]. A popular strategy for indirect methods is based on variance-stabilizing transform (VST) [13] and Gaussian denoiser to recover images polluted by Poisson noise [11]. The most represented indirect method [10] for Poisson denoising uses VST and BM3D denoiser [14] to achieve superior performance. However, the denoising performance of such indirect methods will rapidly deteriorate when they suffer from less photon-counting rate, namely, low intensities [6, 7].

In order to alleviate the deficiency of the above-mentioned indirect methods, some methods discard the VST strategy and directly investigate the statistics of Poisson noise [5–7, 12]. For instance, Kumar *et al*. [6] designed a low-rank approach with weight nuclear norm constraint [15] for Poisson denoising. Zhao *et al*. [7] proposed a nonlocal low-rank-based variational method for removing Poisson noise, which has achieved state-of-the-art performance. However, these methods usually produce annoying visual artifacts due to the aggregation of overlapping patches [16, 17]. Recent studies have suggested that deep convolutional neural networks (CNN) have achieved promising performance for Poisson denoising [5, 18, 19]. For example, Feng *et al*. [5] developed a trainable nonlinear reaction-diffusion (TNRD) model for Poisson denoising. Remez *et al*. [18] proposed a class-aware fully CNN architecture for removing Poisson noise. However, Poisson noise usually arises from various photo-limited imaging systems (*e.g.*, astronomy imaging [2] and spectral imaging [3]), and these deep CNN-based methods trained the denoising model by a standard natural image corpus, leading to a lack of generalizability. Moreover, they only consider utilizing image local property while neglecting image nonlocal self-similarity (NSS) property [17], which may limit their effectiveness.

Bearing the above concern in mind, in this paper, we propose a novel approach using simultaneous nonlocal low-rank and deep priors (SNLDP) for Poisson denoising. The proposed SNLDP simultaneously exploits image NSS and deep image priors under the hybrid plug and play (H-PnP) framework, which contains multiple

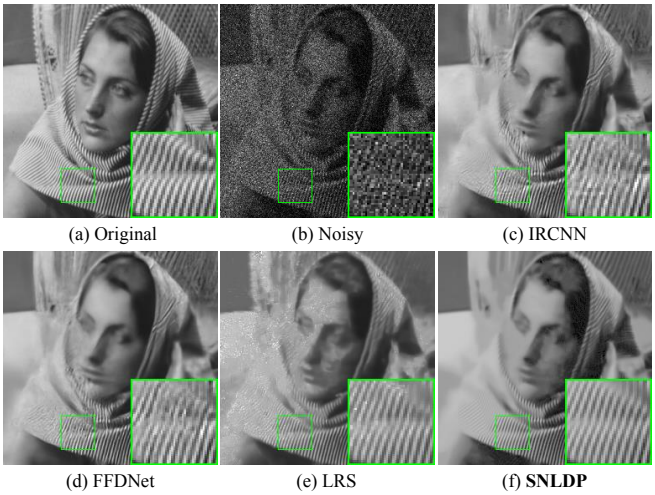

(a) Original (b) Noisy (c) IRCNN
(d) FFDNet (e) LRS (f) **SNLDP**

Fig. 1. Poisson denoising results of *Barbara* with $P = 10$. (a) Original image; (b) Noisy image; (c) IRCNN [8] (PSNR = 24.47dB); (d) FFDNet [9] (PSNR = 24.62dB); (e) LRS [7] (PSNR = 24.63dB); (f) **SNLDP** (PSNR = **25.34dB**).

* Corresponding Author. This research is supported by Academic Research Fund Tier 1 (Project ID: RG137/20), MOE, Singapore.

pairs of complementary priors, namely, *nonlocal* and *local*, *shallow* and *deep*, and *internal* and *external*. The main contributions of this paper are summarized as follows:

1) Based on the H-PnP framework, we propose a highly effective Poisson denoising approach via combing complementary nonlocal low-rank and deep image priors to jointly employ both NSS, scale model richness, and good generalizability.
2) To make the optimization tractable, an effective alternating direction method of multiplier (ADMM) algorithm based on the alternative minimization framework is provided to solve the proposed SNLDP-based Poisson denoising problem.
3) Experimental results verify that the proposed SNLDP outperforms many popular or state-of-the-art Poisson denoising methods both quantitatively and qualitatively. Fig. 1 shows an example of the Poisson denoising result by comparing our proposed SNLDP with three state-of-the-art methods, wherein IRCNN [8] and FFDNet [9] are two deep CNN-based methods accompanied by VST preprocessing, while LRS [7] and our proposed SNLDP are the direct methods by employing the statistics of Poisson noise. We can clearly see that the proposed SNLDP recovers better image details than other competing methods.

2. PRELIMINARIES

In this section, we briefly introduce the Poisson statistics-based plug and play (PnP) model and the nonlocal low-rank model.

2.1. Poisson Statistics-based PnP Model

Poisson denoising aims to recover the latent clean image $\boldsymbol{x} \in \mathbb{R}^N$ from its noisy observation $\boldsymbol{y} \in \mathbb{Z}_+^N$. Each observed pixel value y_i in $\boldsymbol{y}$ is assumed to be a Poisson distributed independent random variable with mean and variance equal to x_i in $\boldsymbol{x}$. Then, the probability distribution function of $\boldsymbol{y}$ can be described as follows,

$$\boldsymbol{P}(\boldsymbol{y}|\boldsymbol{x}) = \begin{cases} \prod_{i=1}^{N} \frac{x_i^{y_i}\exp(-x_i)}{y_i!}, & \text{if } x_i > 0 \\ \delta_0(y_i), & \text{if } x_i = 0 \end{cases} \tag{1}$$

where $\delta_0(\cdot)$ represents the Kronecker delta function, and x_i and y_i are the i-th component in $\boldsymbol{x}$ and $\boldsymbol{y}$, respectively.

Recent studies have demonstrated that the PnP [20] is a promising framework that employs effective Gaussian denoisers to solve general inverse problems, such as Poisson denoising [4], image deblurring [8], and image inpainting [21]. In the Poisson denoising task, the PnP framework first maximizes the probability distribution function Eq. (1) by conducting a maximum a posteriori (MAP) estimator. Following this, the observed model (derived from Eq. (1)) and the Gaussian denoiser are integrated into the variational framework to solve the following MAP problem,

$$\arg\min_{\boldsymbol{x}} < \boldsymbol{x} - \boldsymbol{y}\log\boldsymbol{x}, \boldsymbol{1} > + \lambda\boldsymbol{\Upsilon}(\boldsymbol{x}), \tag{2}$$

where the first term in Eq. (2) is also recognized as the so-called Csiszár I-divergence model [22], which has been widely employed in previous Poisson denoising algorithms [5, 6]. λ is a regularization parameter, and $<,>$ is the standard inner product. $\boldsymbol{\Upsilon}(\cdot)$ represents the regularizer, which relies on appropriate Gaussian denoiser priors [14, 15]. Most recently, the PnP-based approaches exploited the advanced deep denoisers to achieve remarkable performance in various image processing and computational imaging studies [23–26].

2.2. Nonlocal Low-Rank Model

Nonlocal low-rank model groups similar nonlocal patches and exploits the low-rank property of each *patch group*, which has shown great potential in various image restoration applications [15, 27, 28]. To be specific, an image $\boldsymbol{x} \in \mathbb{R}^N$ is first divided into n overlapped patches $\{\boldsymbol{x}_i\}_{i=1}^n \in \mathbb{R}^{b\times 1}$. Following this, taking each $\boldsymbol{x}_i$ as the reference patch, m closest patches are collected for the reference patch $\boldsymbol{x}_i$, which is formed a patch group, *i.e.*, $\boldsymbol{R}_i\boldsymbol{x} = \boldsymbol{X}_i = \{\boldsymbol{x}_{i,1}, \ldots, \boldsymbol{x}_{i,m}\}$, where each $\boldsymbol{R}_i : \boldsymbol{x} \mapsto \boldsymbol{R}_i\boldsymbol{x} \in \mathbb{R}^{b\times m}$ represents a K-Nearest Neighbour (KNN) [29] operator, which is exploited to gather the m closest patches (by calculating Euclidean distance) to the i-th patch from $\boldsymbol{x}$. Since all patches in each patch group $\boldsymbol{R}_i\boldsymbol{x}$ has similar structures, the constructed data matrix possesses the low-rank property [28]. Then, the low-rank matrix $\boldsymbol{L}_i$ can be estimated from each patch group $\boldsymbol{R}_i\boldsymbol{x}$ by solving the following minimization problem,

$$\hat{\boldsymbol{L}}_i = \arg\min_{\boldsymbol{L}_i} \tfrac{1}{2}\|\boldsymbol{R}_i\boldsymbol{x} - \boldsymbol{L}_i\|_F^2 + \lambda\mathcal{D}(\boldsymbol{L}_i) \quad \forall i, \tag{3}$$

where $\mathcal{D}(\boldsymbol{L}_i)$ denotes the regularizer describing the low-rank property of $\boldsymbol{L}_i$, and λ is a positive constant. The popular regularizer $\mathcal{D}(\boldsymbol{L}_i)$ includes nuclear norm [27], weighted nuclear norm [15], and rank residual [28], which has been verified as effective for image restoration. However, such methods inevitably generate visual artifacts because of the aggregation of overlapping patches [16, 17].

3. PROPOSED METHOD

3.1. SNLDP Model for Poisson Denoising

As mentioned above, nonlocal-based methods and deep CNN-based methods have their respective advantages and shortcomings. In this subsection, we propose a general hybrid PnP (H-PnP) framework for highly effective Poisson denoising by fusing the complementary nonlocal low-rank and deep image priors, which jointly employ both NSS, scale model richness, and good generalizability. More specifically, the nonlocal low-rank and deep denoiser priors are integrated into the regularization-based framework (2), which are regarded as the dual regularizers in the following SNLDP problem,

$$\begin{aligned}(\hat{\boldsymbol{x}}, \hat{\boldsymbol{L}}_i) = &\arg\min_{\boldsymbol{x},\boldsymbol{L}_i} < \boldsymbol{x} - \boldsymbol{y}\log\boldsymbol{x}, \boldsymbol{1} > \\ &+ \tfrac{1}{2\rho}\textstyle\sum_{i=1}^n \|\boldsymbol{R}_i\boldsymbol{x} - \boldsymbol{L}_i\|_F^2 + \lambda\sum_{i=1}^n \mathcal{D}(\boldsymbol{L}_i) + \tau\boldsymbol{\Upsilon}(\boldsymbol{x}),\end{aligned} \tag{4}$$

where $\boldsymbol{\Upsilon}(\boldsymbol{x})$ denotes the deep denoiser to regularize the entire image $\boldsymbol{x}$ with effectively preserving the fine image details. ρ is the balancing factor to make (4) more feasible. Apparently, compared to the traditional nonlocal low-rank or deep image models, the proposed SNLDP incorporates two complementary priors under the H-PnP framework, which assumes that the underlying image $\boldsymbol{x}$ meets both low-rank and deep priors. We will demonstrate that the proposed SNLDP can achieve better results than many existing single prior-based Poisson denoising algorithms in the experiments (See Section 4 for more details).

3.2. Optimization for the SNLDP Problem

In this subsection, to make the optimization tractable, we present an effective ADMM algorithm [30] under the alternative minimizing framework to solve the proposed SNLDP problem. To be concrete, the algorithm first alternates solving Eq. (4) by $\boldsymbol{L}_i$ and $\boldsymbol{x}$, corresponding to low-rank matrix approximation and image update subproblem. Following this, we employ the ADMM algorithm to solve the image update sub-problem.

3.2.1. Low-Rank Matrix Approximation: $\boldsymbol{L}_i$ Sub-Problem

For fixed $\boldsymbol{x}$, the low-rank $\boldsymbol{L}_i$ sub-problem in Eq. (4) becomes,

$$\hat{\boldsymbol{L}}_i = \arg\min_{\boldsymbol{L}_i} \tfrac{1}{2}\|\boldsymbol{R}_i\boldsymbol{x} - \boldsymbol{L}_i\|_F^2 + \rho\lambda\mathcal{D}(\boldsymbol{L}_i), \quad \forall i. \tag{5}$$

It is worth noting that the low-rank regularizer $\mathcal{D}(\boldsymbol{L}_i)$ is not specified. In this paper, we adopt a weighted nuclear norm minimization (WNNM) [15] to describe the low-rank property of $\boldsymbol{L}_i$, which has demonstrated superior performance for various image restoration studies [31, 32]. There exists a closed-form solution of $\hat{\boldsymbol{L}}_i$ by performing the WNNM algorithm [15]. Due to the limited pages, more details about the WNNM algorithm, please refer to [15].

3.2.2. Image Update: $\boldsymbol{x}$ Sub-Problem

For fixed $\boldsymbol{L}_i$, the image $\boldsymbol{x}$ can be updated by solving the following problem,

$$\hat{\boldsymbol{x}} = \arg\min_{\boldsymbol{x}} < \boldsymbol{x} - \boldsymbol{y}\log\boldsymbol{x}, \boldsymbol{1} > + \tfrac{1}{2\rho}\textstyle\sum_{i=1}^{n}\|\boldsymbol{R}_i\boldsymbol{x} - \boldsymbol{L}_i\|_F^2 + \tau\boldsymbol{\Upsilon}(\boldsymbol{x}). \tag{6}$$

One can observe that we directly solve Eq. (6) seems to be difficult because of a non-convex deep image regularizer $\boldsymbol{\Upsilon}(\boldsymbol{x})$. Therefore, to facilitate the optimization, we exploit an effective ADMM algorithm [30] to solve Eq. (6). To be specific, we first present an auxiliary variable $\boldsymbol{z} = \boldsymbol{x}$ and then request the ADMM algorithm; the image update sub-problem is now transformed into three iterative steps:

$$\hat{\boldsymbol{x}} \leftarrow \arg\min_{\boldsymbol{x}} < \boldsymbol{x} - \boldsymbol{y}\log\boldsymbol{x}, \boldsymbol{1} > + \tfrac{1}{2\rho}\textstyle\sum_{i=1}^{n}\|\boldsymbol{R}_i\boldsymbol{x} - \boldsymbol{L}_i\|_F^2 + \tfrac{\alpha}{2}\|\boldsymbol{x} - \boldsymbol{z} + \tfrac{\boldsymbol{p}}{\alpha}\|_2^2, \tag{7}$$

$$\hat{\boldsymbol{z}} \leftarrow \arg\min_{\boldsymbol{z}} \tfrac{\alpha}{2}\|\boldsymbol{x} - \boldsymbol{z} + \tfrac{\boldsymbol{p}}{\alpha}\|_2^2 + \tau\boldsymbol{\Upsilon}(\boldsymbol{z}), \tag{8}$$

$$\hat{\boldsymbol{p}} \leftarrow \boldsymbol{p} - \alpha(\boldsymbol{x} - \boldsymbol{z}), \tag{9}$$

where $\boldsymbol{p}$ represents the Lagrangian multiplier, and α is the balancing factor. It can be seen that the image update problem is transformed into solving two sub-problems, *i.e.*, $\boldsymbol{x}$ and $\boldsymbol{z}$ sub-problem. We introduce how to solve them to obtain an efficient solution below.

$\boldsymbol{z}$ Sub-Problem:

Given $\boldsymbol{x}$ and $\boldsymbol{p}$, $\boldsymbol{z}$ sub-problem in Eq. (8) can be rewritten as,

$$\hat{\boldsymbol{z}} = \arg\min_{\boldsymbol{z}} \tfrac{1}{2(\sqrt{\tau/\alpha})^2}\|\boldsymbol{g} - \boldsymbol{z}\|_2^2 + \boldsymbol{\Upsilon}(\boldsymbol{z}), \tag{10}$$

where $\boldsymbol{g} = \boldsymbol{x} + \frac{\boldsymbol{p}}{\alpha}$. From the perspective of MAP, solving $\boldsymbol{z}$ is usually treated as a Gaussian denoising problem with the noise standard deviation being $\sqrt{\tau/\alpha}$. Thus, the solution of such denoising problems can be described as follows,

$$\hat{\boldsymbol{z}} = \mathcal{H}(\boldsymbol{g}, \sqrt{\tau/\alpha}), \tag{11}$$

where $\mathcal{H}(\cdot)$ represents a Gaussian denoiser based on the specific image prior $\boldsymbol{\Upsilon}(\cdot)$. In general, we can employ any Gaussian denoiser to approach $\mathcal{H}(\cdot)$. This paper adopts a fast and flexible denoising CNN (FFDNet) method [9] as the Gaussian denoiser for solving Eq. (11), which not only handles different noise standard deviation adaptively but also complementarities with the nonlocal low-rank prior.

In order to expediently solve the $\boldsymbol{x}$ sub-problem in Eq. (7), we continue to use the ADMM algorithm to solve it, and we introduce another auxiliary variable $\boldsymbol{s} = \boldsymbol{x}$. Then, we invoke the ADMM algorithm, and the optimization for Eq. (7) is transformed into the following steps:

$$\hat{\boldsymbol{x}} \leftarrow \arg\min_{\boldsymbol{x}} < \boldsymbol{x} - \boldsymbol{y}\log\boldsymbol{x}, \boldsymbol{1} > + \tfrac{\alpha}{2}\|\boldsymbol{x} - \boldsymbol{z} + \tfrac{\boldsymbol{p}}{\alpha}\|_2^2 + \tfrac{\beta}{2}\|\boldsymbol{x} - \boldsymbol{s} + \tfrac{\boldsymbol{q}}{\beta}\|_2^2, \tag{12}$$

$$\hat{\boldsymbol{s}} \leftarrow \arg\min_{\boldsymbol{s}} \tfrac{1}{2\rho}\textstyle\sum_{i=1}^{n}\|\boldsymbol{R}_i\boldsymbol{s} - \boldsymbol{L}_i\|_F^2 + \tfrac{\beta}{2}\|\boldsymbol{x} - \boldsymbol{s} + \tfrac{\boldsymbol{q}}{\beta}\|_2^2, \tag{13}$$

$$\hat{\boldsymbol{q}} \leftarrow \boldsymbol{q} - \beta(\boldsymbol{x} - \boldsymbol{s}), \tag{14}$$

Algorithm 1 Proposed SNLDP Algorithm for Poisson denoising.

Require: The noisy image $\boldsymbol{y}$, the deep Gaussian denoiser $\mathcal{H}(\cdot)$ and parameters $b, m, \rho, \lambda, \tau, \alpha, \beta$.

1: **Initialization:** Estimate an initial image $\hat{\boldsymbol{x}}^{(0)} = \boldsymbol{y}$.
2: **for** $t = 1$ to Max-Iter **do**
3: Divide $\hat{\boldsymbol{x}}^{(t)}$ into n overlapping patches $\{\hat{\boldsymbol{x}}_i\}_{i=1}^{N}$ with size $\sqrt{b} \times \sqrt{b}$;
4: **for** Each patch $\hat{\boldsymbol{x}}_i$ in $\hat{\boldsymbol{x}}^{(t)}$ **do**
5: Find m nonlocal similar patches to form a patch group $\boldsymbol{R}_i\boldsymbol{x}$ via the KNN algorithm [29];
6: Update $\hat{\boldsymbol{L}}_i$ by solving Eq. (5);
7: **end for**
8: **ADMM:**
9: Initialization: $\boldsymbol{p} = 0; \boldsymbol{q} = 0; \boldsymbol{z} = \hat{\boldsymbol{x}}^t; \boldsymbol{s} = \hat{\boldsymbol{x}}^t$
10: Update $\hat{\boldsymbol{z}}$ by solving Eq. (11);
11: Update $\hat{\boldsymbol{s}}$ by solving Eq. (15);
12: Update $\hat{\boldsymbol{x}}$ by solving Eq. (18);
13: Update $\hat{\boldsymbol{p}}$ by solving Eq. (9);
14: Update $\hat{\boldsymbol{q}}$ by solving Eq. (14);
15: **end for**
16: **Output:** The final denoised image $\hat{\boldsymbol{x}}$.

Fig. 2. The eight widely used images in our experiments.

where $\boldsymbol{q}$ and β are the Lagrangian multiplier and the balancing factor, respectively. It is clear that Eq. (12) and Eq. (13) are employed to solve the $\boldsymbol{x}$ and $\boldsymbol{s}$ sub-problem, respectively.

$\boldsymbol{s}$ Sub-Problem:

Given $\boldsymbol{x}$, $\boldsymbol{L}_i$ and $\boldsymbol{q}$, we can clearly observe that Eq. (13) is a quadratic optimization problem, which admits a closed-form solution, namely,

$$\hat{\boldsymbol{s}} = \left(\textstyle\sum_{i=1}^{n}\boldsymbol{R}_i^T\boldsymbol{R}_i + \rho\beta\boldsymbol{I}\right)^{-1}\left(\textstyle\sum_{i=1}^{n}\boldsymbol{R}_i^T\boldsymbol{L}_i + \rho\beta\boldsymbol{x} + \rho\boldsymbol{q}\right), \tag{15}$$

where $\boldsymbol{I}$ is an identity matrix, $\boldsymbol{R}_i^T\boldsymbol{R}_i = \Sigma_{j=1}^{m}\boldsymbol{R}_{i,j}^T\boldsymbol{R}_{i,j}$, and $\boldsymbol{R}_i^T\boldsymbol{L}_i = \Sigma_{j=1}^{m}\boldsymbol{R}_{i,j}^T\boldsymbol{L}_{i,j}$. Note that the $\boldsymbol{s}$ sub-problem can be solved efficiently by element-wise division since $(\sum_{i=1}^{n}\boldsymbol{R}_i^T\boldsymbol{R}_i + \rho\beta\boldsymbol{I})$ is a diagonal matrix essentially.

$\boldsymbol{x}$ Sub-Problem:

Given $\boldsymbol{z}, \boldsymbol{s}, \boldsymbol{p}$, and $\boldsymbol{q}$, we can see that Eq. (12) leads to a point-wise solution for each component individually and is given by,

$$\arg\min_{x_i}(x_i - y_i\log x_i) + \frac{\alpha}{2}(x_i - z_i + \frac{p_i}{\alpha})^2 + \frac{\beta}{2}(x_i - s_i + \frac{q_i}{\beta})^2, \tag{16}$$

where d_i denotes the i-th component of the arbitrary $\boldsymbol{d}$. The solution of Eq. (16) can be obtained by setting the gradient to zero, and therefore we can obtain the following quadratic equation,

$$(\alpha + \beta)x_i^2 - (\alpha z_i + \beta s_i - p_i - q_i - 1)x_i - y_i = 0. \tag{17}$$

It can be seen that the solution of Eq. (17) possesses two real roots, and we select the positive one because of the constraint of $x_i > 0$. Therefore, the solution of Eq. (16) can be obtained as follows,

$$\hat{x}_i = \frac{r_i + \sqrt{r_i^2 + 4(\alpha + \beta)y_i}}{2(\alpha + \beta)}, \tag{18}$$

where $r_i = \alpha z_i + \beta s_i - p_i - q_i - 1$.

Table 1. PSNR (dB) comparison of different methods for Poisson denoising.

	$P = 10$								$P = 15$							
Methods	**BM3D**	**PURE-LET**	**Dn-CNN**	**IRCNN**	**FFDNet**	**LRPD**	**LRS**	**SNLDP**	**BM3D**	**PURE-LET**	**Dn-CNN**	**IRCNN**	**FFDNet**	**LRPD**	**LRS**	**SNLDP**
Baboon	21.61	20.88	20.54	21.96	22.02	22.30	22.42	**23.07**	22.27	21.25	22.06	22.63	22.71	22.87	22.98	**23.73**
Barbara	25.08	23.07	22.38	24.47	24.62	24.21	24.63	**25.34**	26.19	23.83	25.32	25.46	25.63	24.71	25.89	**26.63**
boats	25.24	23.57	25.03	25.26	25.69	24.75	25.29	**25.86**	26.49	24.54	26.24	26.60	26.95	24.98	26.41	**27.16**
J. Bean	26.93	25.11	25.57	27.18	27.64	26.27	27.63	**28.50**	28.26	25.32	28.07	28.49	29.05	27.27	28.98	**29.74**
Tank	25.87	25.17	24.98	25.90	26.07	27.07	27.21	**27.59**	26.39	25.30	26.30	26.52	26.65	27.08	27.87	**28.03**
Peppers	25.50	23.89	24.80	25.92	**26.12**	24.19	24.97	25.98	26.29	23.70	26.81	26.86	26.90	24.82	26.08	**26.95**
Straw	20.68	19.55	18.24	20.88	21.17	19.98	20.62	**21.40**	21.60	20.07	21.10	21.91	**22.14**	21.45	21.55	21.93
Flag	25.72	21.64	23.08	25.75	25.90	22.04	24.33	**26.36**	26.88	22.34	26.53	27.10	27.18	23.48	25.92	**27.55**
Average	24.58	22.86	23.08	24.66	24.90	23.85	24.64	**25.51**	25.55	23.29	25.30	25.70	25.90	24.58	25.71	**26.46**
	$P = 20$								$P = 30$							
Methods	**BM3D**	**PURE-LET**	**Dn-CNN**	**IRCNN**	**FFDNet**	**LRPD**	**LRS**	**SNLDP**	**BM3D**	**PURE-LET**	**Dn-CNN**	**IRCNN**	**FFDNet**	**LRPD**	**LRS**	**SNLDP**
Baboon	22.79	21.34	21.94	23.21	23.36	23.46	23.51	**24.15**	23.62	22.62	21.70	24.10	24.15	24.41	24.11	**24.89**
Barbara	27.02	23.85	25.11	26.30	26.42	25.61	26.60	**27.65**	28.07	24.96	25.01	27.20	27.42	26.90	27.79	**28.82**
boats	27.04	24.99	26.34	27.14	27.42	25.87	27.26	**27.93**	28.20	24.55	26.36	27.98	28.50	27.19	28.39	**28.97**
J. Bean	29.17	25.73	28.58	28.97	29.90	28.13	29.69	**30.72**	30.31	27.89	28.57	30.48	30.88	29.38	30.90	**31.84**
Tank	26.86	25.38	26.33	26.95	27.06	27.79	28.27	**28.61**	27.48	24.44	26.10	27.48	27.66	28.07	28.81	**29.17**
Peppers	26.93	23.75	26.82	27.49	27.48	25.84	26.84	**27.69**	27.85	24.42	26.80	28.34	28.36	27.16	27.95	**28.43**
Straw	22.29	20.56	21.58	22.68	22.83	22.10	22.21	**22.88**	23.27	21.94	21.14	23.60	23.85	23.43	23.14	**24.01**
Flag	27.99	22.82	27.70	28.21	28.44	25.11	27.26	**28.69**	28.96	25.19	26.97	**29.62**	29.44	27.24	28.72	29.33
Average	26.26	23.55	25.55	26.37	26.61	25.49	26.46	**27.29**	27.22	24.50	25.33	27.35	27.53	26.72	27.47	**28.18**

Until now, we have obtained an efficient solution for each subproblem via the ADMM algorithm based on the alternating minimization framework, making the proposed SNLDP-based Poisson denoising algorithm more stable and practical. The complete description of the proposed SNLDP-based Poisson denoising method are summarized in Algorithm 1.

4. EXPERIMENTAL RESULTS

In this section, we conduct several experiments to verify the effectiveness of the proposed SNLDP-based Poisson denoising algorithm. The peak signal-to-noise ratio (PSNR) is used as the quantitative quality metric to evaluate the performance of different algorithms. Since Poisson denoising is signal-dependent, the noise levels of the degraded images are dependent on the peak pixel intensity P. Due to the limited pages, this paper has only considered four different noise levels: the peak pixel intensities of the images with P = 10, 15, 20, and 30. The basic parameters of the proposed SNLDP-based Poisson denoising algorithm are set as follows. The size of patch b is set to 49×1, and the number of nonlocal simiar patches m is set to 80. α is set to 0.005, and β is set to 0.009. ρ is set to 0.2, 0.4 and 0.5 for $P \leq 10$, $10 < P \leq 20$ and $P > 20$, respectively. The source code of the proposed SNLDP-based Poisson denoising algorithm is available at: https://drive.google.com/file/d/14fLnU6Q-Vz3gPXAiKquy2_nttRQQgiy9/view?usp=sharing.

In this paper, we compare the proposed SNLDP with seven popular or state-of-the-art approaches, including BM3D [10], PURE-LET [33], Dn-CNN [34], IRCNN [8], FFDNet [9], LRPD [6], and LRS [7]. It is worth noting that BM3D, PURE-LET, Dn-CNN, IRCNN and FFDNet are indirect methods accompanied by VST preprocessing, while LRPD, LRS and the proposed SNLDP are direct methods exploiting the statistics of Poisson noise. In addition, Dn-CNN, IRCNN and FFDNet are three deep CNN-based Gaussian denoising methods. LRPD relies on the WNNM algorithm [15], which is still a state-of-the-art method for Gaussian denoising. LRS is a recently direct Poisson denoising approach, which has state-of-the-art performance. We evaluate the performance of all competing methods via eight widely used images, whose scenes are shown in Fig. 2. The PSNR comparison results of all methods are shown in Table 1, with the best results highlighted in bold. An overall impression observed from Table 1 is that the proposed SNLDP achieves the highest PSNR values in almost all cases. On average, the PSNR gains of the proposed SNLDP over BM3D, PURE-LET, Dn-CNN, IRCNN, FFDNet, LRPD and LRS are 0.96dB, 3.31dB, 2.05dB, 0.84dB, 0.62dB, 1.70dB and 0.79dB, respectively.

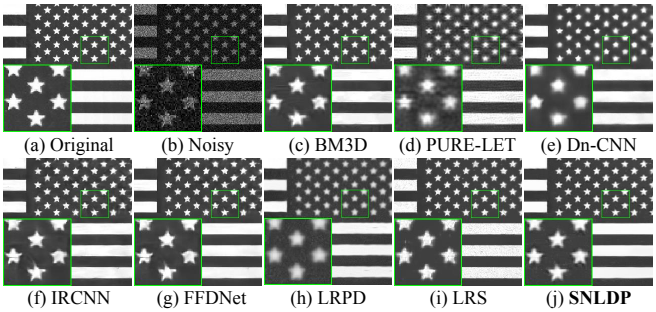

Fig. 3. Poisson denoising results of *Flag* with P = 10. (a) Original image; (b) Noisy image; (c) BM3D [10] (PSNR = 25.72dB); (d) PURE-LET [33] (PSNR = 21.64dB); (e) Dn-CNN [34] (PSNR = 23.08dB); (f) IRCNN [8] (PSNR = 25.75dB); (g) FFDNet [9] (PSNR = 25.90dB); (h) LRPD [6] (PSNR = 22.04dB); (i) LRS [7] (PSNR = 24.33dB); (j) **SNLDP** (PSNR = **26.36dB**).

The visual comparison results of all methods are shown in Fig. 3. It can be seen that PUR-LET, Dn-CNN, and LRPD methods produce blur effects, while IRCNN and FFDNet methods are prone to generate undesirable visual artifacts. Although the LRS method obtains decent visible results, there are still residing some noises. In contrast, the proposed SNLDP approach not only effectively removes the Poisson noise but also preserves more fine image details.

5. CONCLUSION

This paper has proposed a novel SNLDP approach for Poisson denoising. The proposed SNLDP has simultaneously employed nonlocal low-rank and deep image priors under the H-PnP framework, which comprises multiple pairs of complementary priors, namely, nonlocal and local, shallow and deep, and internal and external. Furthermore, we have provided an effective ADMM algorithm based on the alternative minimization framework to solve the SNLDP-based Poisson denoising problem. Experimental results have demonstrated that the proposed SNLDP outperforms many popular or state-of-the-art Poisson denoising methods in terms of objective and visual quality.

References

[1] W. Liu and W. Lin, "Additive white gaussian noise level estimation in svd domain for images," *IEEE Transactions on Image Processing*, vol. 22, no. 3, pp. 872–883, 2013.

[2] J. Schmitt, J. Starck, J. Casandjian, J. Fadili, and I. Grenier, "Poisson denoising on the sphere: application to the fermi gamma ray space telescope," *Astronomy & Astrophysics*, vol. 517, p. A26, 2010.

[3] W. Dong, T. Huang, G. Shi, Y. Ma, and X. Li, "Robust tensor approximation with laplacian scale mixture modeling for multiframe image and video denoising," *IEEE Journal of Selected Topics in Signal Processing*, vol. 12, no. 6, pp. 1435–1448, 2018.

[4] A. Rond, R. Giryes, and M. Elad, "Poisson inverse problems by the plug-and-play scheme," *Journal of Visual Communication and Image Representation*, vol. 41, pp. 96–108, 2016.

[5] W. Feng, P. Qiao, and Y. Chen, "Fast and accurate poisson denoising with trainable nonlinear diffusion," *IEEE Transactions on Cybernetics*, vol. 48, no. 6, pp. 1708–1719, 2018.

[6] P. K. G. and R. R. Sahay, "Low rank poisson denoising (lrpd): A low rank approach using split bregman algorithm for poisson noise removal from images," in *2019 IEEE/CVF Conference on Computer Vision and Pattern Recognition Workshops (CVPRW)*, 2019, pp. 1907–1916.

[7] M. Zhao, Y.-W. Wen, M. Ng, and H. Li, "A nonlocal low rank model for poisson noise removal," *Inverse Problems & Imaging*, vol. 15, no. 3, p. 519, 2021.

[8] K. Zhang, W. Zuo, S. Gu, and L. Zhang, "Learning deep cnn denoiser prior for image restoration," in *2017 IEEE Conference on Computer Vision and Pattern Recognition (CVPR)*, 2017, pp. 2808–2817.

[9] K. Zhang, W. Zuo, and L. Zhang, "Ffdnet: Toward a fast and flexible solution for cnn-based image denoising," *IEEE Transactions on Image Processing*, vol. 27, no. 9, pp. 4608–4622, 2018.

[10] M. Makitalo and A. Foi, "Optimal inversion of the anscombe transformation in low-count poisson image denoising," *IEEE Transactions on Image Processing*, vol. 20, no. 1, pp. 99–109, 2011.

[11] L. Azzari and A. Foi, "Variance stabilization for noisy+estimate combination in iterative poisson denoising," *IEEE Signal Processing Letters*, vol. 23, no. 8, pp. 1086–1090, 2016.

[12] J. Salmon, Z. Harmany, C.-A. Deledalle, and R. Willett, "Poisson noise reduction with non-local pca," *Journal of mathematical imaging and vision*, vol. 48, no. 2, pp. 279–294, 2014.

[13] M. Makitalo and A. Foi, "A closed-form approximation of the exact unbiased inverse of the anscombe variance-stabilizing transformation," *IEEE Transactions on Image Processing*, vol. 20, no. 9, pp. 2697–2698, 2011.

[14] K. Dabov, A. Foi, V. Katkovnik, and K. Egiazarian, "Image denoising by sparse 3-d transform-domain collaborative filtering," *IEEE Transactions on Image Processing*, vol. 16, no. 8, pp. 2080–2095, 2007.

[15] S. Gu, L. Zhang, W. Zuo, and X. Feng, "Weighted nuclear norm minimization with application to image denoising," in *2014 IEEE Conference on Computer Vision and Pattern Recognition*, 2014, pp. 2862–2869.

[16] Z. Zha, B. Wen, X. Yuan, J. T. Zhou, J. Zhou, and C. Zhu, "Triply complementary priors for image restoration," *IEEE Transactions on Image Processing*, vol. 30, pp. 5819–5834, 2021.

[17] Z. Zha, B. Wen, X. Yuan, J. Zhou, and C. Zhu, "Image restoration via reconciliation of group sparsity and low-rank models," *IEEE Transactions on Image Processing*, vol. 30, pp. 5223–5238, 2021.

[18] T. Remez, O. Litany, R. Giryes, and A. M. Bronstein, "Class-aware fully convolutional gaussian and poisson denoising," *IEEE Transactions on Image Processing*, vol. 27, no. 11, pp. 5707–5722, 2018.

[19] M. Zhang, F. Zhang, Q. Liu, and S. Wang, "Vst-net: variance-stabilizing transformation inspired network for poisson denoising," *Journal of Visual Communication and Image Representation*, vol. 62, pp. 12–22, 2019.

[20] S. V. Venkatakrishnan, C. A. Bouman, and B. Wohlberg, "Plug-and-play priors for model based reconstruction," in *2013 IEEE Global Conference on Signal and Information Processing*, 2013, pp. 945–948.

[21] T. Tirer and R. Giryes, "Image restoration by iterative denoising and backward projections," *IEEE Transactions on Image Processing*, vol. 28, no. 3, pp. 1220–1234, 2019.

[22] I. Csiszar, "Why least squares and maximum entropy? an axiomatic approach to inference for linear inverse problems," *The annals of statistics*, vol. 19, no. 4, pp. 2032–2066, 1991.

[23] Y. Sun, B. Wohlberg, and U. S. Kamilov, "An online plug-and-play algorithm for regularized image reconstruction," *IEEE Transactions on Computational Imaging*, vol. 5, no. 3, pp. 395–408, 2019.

[24] E. Ryu, J. Liu, S. Wang, X. Chen, Z. Wang, and W. Yin, "Plug-and-play methods provably converge with properly trained denoisers," in *Proceedings of the 36th International Conference on Machine Learning*, ser. Proceedings of Machine Learning Research, K. Chaudhuri and R. Salakhutdinov, Eds., vol. 97. PMLR, 09–15 Jun 2019, pp. 5546–5557.

[25] X. Yuan, Y. Liu, J. Suo, and Q. Dai, "Plug-and-play algorithms for large-scale snapshot compressive imaging," in *2020 IEEE/CVF Conference on Computer Vision and Pattern Recognition (CVPR)*, 2020, pp. 1444–1454.

[26] R. Ahmad, C. A. Bouman, G. T. Buzzard, S. Chan, S. Liu, E. T. Reehorst, and P. Schniter, "Plug-and-play methods for magnetic resonance imaging: Using denoisers for image recovery," *IEEE Signal Processing Magazine*, vol. 37, no. 1, pp. 105–116, 2020.

[27] H. Ji, C. Liu, Z. Shen, and Y. Xu, "Robust video denoising using low rank matrix completion," in *2010 IEEE Computer Society Conference on Computer Vision and Pattern Recognition*, 2010, pp. 1791–1798.

[28] Z. Zha, X. Yuan, B. Wen, J. Zhou, J. Zhang, and C. Zhu, "From rank estimation to rank approximation: Rank residual constraint for image restoration," *IEEE Transactions on Image Processing*, vol. 29, pp. 3254–3269, 2020.

[29] J. M. Keller, M. R. Gray, and J. A. Givens, "A fuzzy k-nearest neighbor algorithm," *IEEE Transactions on Systems, Man, and Cybernetics*, vol. SMC-15, no. 4, pp. 580–585, 1985.

[30] S. Boyd, N. Parikh, and E. Chu, *Distributed optimization and statistical learning via the alternating direction method of multipliers*. Now Publishers Inc, 2011.

[31] S. Gu, Q. Xie, D. Meng, W. Zuo, X. Feng, and L. Zhang, "Weighted nuclear norm minimization and its applications to low level vision," *International journal of computer vision*, vol. 121, no. 2, pp. 183–208, 2017.

[32] J. Xu, L. Zhang, D. Zhang, and X. Feng, "Multi-channel weighted nuclear norm minimization for real color image denoising," in *2017 IEEE International Conference on Computer Vision (ICCV)*, 2017, pp. 1105–1113.

[33] F. Luisier, T. Blu, and M. Unser, "Image denoising in mixed poissoncgaussian noise," *IEEE Transactions on Image Processing*, vol. 20, no. 3, pp. 696–708, 2011.

[34] K. Zhang, W. Zuo, Y. Chen, D. Meng, and L. Zhang, "Beyond a gaussian denoiser: Residual learning of deep cnn for image denoising," *IEEE Transactions on Image Processing*, vol. 26, no. 7, pp. 3142–3155, 2017.